Article

A Green Approach to Preparing Vaterite CaCO₃ for Clean Utilization of Steamed Ammonia Liquid Waste and CO₂ Mineralization

Xuewen Song [1], Yuxin Tuo [1], Dan Li [1], Xinrui Hua [1], Ruomeng Wang [1], Jiwei Xue [1], Renhe Yang [2], Xianzhong Bu [1] and Xianping Luo [1,3,*]

[1] School of Resources Engineering, Xi'an University of Architecture and Technology, Xi'an 710055, China; songxwhl@163.com (X.S.); ttuoyuxin@163.com (Y.T.); lidan010312@163.com (D.L.); huaxinrui34@163.com (X.H.); 13061352831@163.com (R.W.); xjw635171816@outlook.com (J.X.); buxianzhong@xauat.edu.cn (X.B.)

[2] State Key Laboratory of Solid Waste Reuse for Building Materials, Beijing Building Materials Academy of Sciences Research, Beijing 100041, China; yangrenhe@xauat.edu.cn

[3] School of Resources and Environmental Engineering, Jiangxi University of Science and Technology, Ganzhou 341000, China

* Correspondence: luoxianping9491@163.com

Abstract: In the salt lake industry, large amounts of steamed ammonia liquid waste are discharged as byproducts. The conversion of the residues into high value-added vaterite-phase calcium carbonate products for industrial applications is highly desirable. In this research, the feasibility of preparing vaterite-phase $CaCO_3$ in different $CaCl_2$-CO_2-MOH-H_2O systems using steamed ammonia liquid waste was studied in the absence of additives. The effects of initial $CaCl_2$ concentration, stirring speed and CO_2 flow rate on the composition of the $CaCO_3$ crystal phase were investigated. The contents of vaterite were researched by the use of steamed ammonia liquid waste as a calcium source and pure calcium chloride as a contrast. The influence of the concentration of $C_{NH_3 \cdot H_2O}/C_{Ca^{2+}}$ on the carbonation ratio and crystal phase composition was studied. The reaction conditions on the content, particle size and morphology of vaterite influence were discussed. It was observed that single vaterite-phase $CaCO_3$ was favored in the $CaCl_2$-CO_2-NH_4OH-H_2O system. Additionally, the impurity ions in steamed ammonia liquid waste play a key role in the nucleation and crystallization of vaterite, which could affect the formation of single-phase vaterite. The obtained results provided a novel method for the preparation of single vaterite particles with the utilization of CO_2 and offered a selective method for the extensive utilization of steamed ammonia liquid waste.

Keywords: calcium carbonate; vaterite; CO_2; steamed ammonia liquid waste

1. Introduction

Steamed ammonia liquid waste is a byproduct produced in the process of preparing magnesium hydroxide from waste bischofite in salt lakes [1]. After using limestone to produce ammonia gas, the suspended solids are sedimented. The overflow, containing $CaCl_2$, is discharged due to ineffective methods; now, millions of tons of steamed ammonia liquid waste are produced yearly. A large amount of the industrial waste discharged cannot be recycled reasonably, and most of it is landfilled, causing a waste of calcium resources and serious environmental pollution. Consequently, designing a specific scientific approach to carrying out the recovery and utilization of $CaCl_2$ in steamed ammonia liquid waste is scientifically relevant.

Massive CO_2 emissions are generated by the continuous development of the world's industry [2]; the increasing global CO_2 concentration has caused great harm to the world's climate security [3,4]. According to the policy plan of the People's Republic of China, the carbon peak should be achieved by 2030, and efforts should be made to achieve carbon

neutrality by 2060 [5]. The International Panel on Climate Change (IPCC) also proposed that to stabilize the concentration of CO_2 in the atmosphere, global greenhouse gas (GHG) emissions must be reduced by as much as 80% by 2050 [6]. For this reason, the scientific community is researching key steps to reducing CO_2 emission and developing systems for capturing, storing and utilizing CO_2 [7–11]. It is well known that indirect carbonation is a typical carbon capture, utilization and storage technology. However, it is very difficult to achieve the large-scale application of this technology because of high cost, high energy consumption and some other issues [12].

Calcium carbonate ($CaCO_3$) is a substance widely distributed in the Earth's lithosphere and biosphere and has many advantages, so it is generally used as a stuffing and reinforcing agent for coating paper, ink, textile, rubber and plastics [13–16], and it has the same nutritive applications in toothpaste, food, medicine and feed [17]. There have been some studies on the production of $CaCO_3$ products from industrial byproducts, such as oyster shells [18], gypsum [19–21], carbide slag [22,23] and industrial alkali [24–27]. Using CO_2 as a carbon source for the preparation of $CaCO_3$ products is a hot topic in the scientific community [28,29]. The production of valuable products in the process of eliminating CO_2 can significantly improve the economic competitiveness of technology. Using waste as calcium and CO_2 as a carbon source, preparing $CaCO_3$ products via carbonization is also a hot topic in the scientific community [30,31]. $CaCO_3$ has three different anhydrous polymorphs: calcite, aragonite and vaterite [32]. Vaterite is the most metastable phase of $CaCO_3$ and can easily transform into calcite or aragonite under ambient environmental conditions. However, it has a higher specific surface area, higher solubility, higher dispersibility and smaller specific gravity compared to calcite and aragonite, so it is anticipated to be used for various intentions [33–37]. Due to its poor thermal stability and difficulty in obtaining an extremely special and excellent property, the preparation of vaterite is also a hot topic at present [38,39]. At the same time, using waste as a calcium source and CO_2 as a carbon source, prepared $CaCO_3$ products are usually calcitic or partially contain calcite and cannot be used to obtain vaterite $CaCO_3$. There are few studies on synthesizing metastable vaterite, which usually requires auxiliary processes, such as ultrasound. Hence, exploratory research on the preparation of vaterite products using the mineralization method on steamed ammonia waste liquid would be a pioneering achievement. In this paper, we fabricated single-vaterite $CaCO_3$ using steamed ammonia waste liquid as the calcium source via a carbonation route, and the synthesis parameters influencing the vaterite phase, particle size and shape without additives were researched. According to our best knowledge, no one has ever carried out a comprehensive research project on the topic of the production of metastable vaterite through the process of carbonization utilizing distilled industrial ammonia waste liquid in the absence of additives and auxiliary procedures.

In the present work, the feasibility of preparing vaterite $CaCO_3$ crystals in different systems using steamed ammonia liquid waste via a carbonation route was studied first. On the basis of proving that the system of $CaCl_2$-CO_2-NH_4OH-H_2O of steamed ammonia liquid waste is conducive to the formation of vaterite, pure calcium chloride and steamed ammonia liquid waste were analyzed as calcium sources, and the effect of the concentration of $CaCl_2$ solution (using different calcium sources), stirring speed, and CO_2 flow rate on the shape, size and content of vaterite in $CaCO_3$ particles was researched without any additives at atmospheric temperature. The effect of preparation conditions on the percentage of vaterite content of the particles derived was enforced using reaction surface methodology. The particle size, microstructure and morphology of the synthesized vaterite $CaCO_3$ were characterized using X-ray diffraction (XRD), Fourier transform infrared (FTIR) spectroscopy, scanning electron microscopy (SEM) and laser particle size analysis (LPSA) techniques. In this study, single crystal-phase vaterite particles were prepared via the carbonation route using industrial byproducts as a calcium source. This research can help in achieving energy saving, emission reduction and the solidification of CO_2, and developing a more feasible method for realizing the preparation of vaterite particles, promoting the process of industrial vaterite production, and expanding the application scope of vaterite.

2. Material and Methods

2.1. Raw Material

The steamed ammonia liquid waste was collected from Qinghai West Magnesium Industry Co., Ltd. in Qinghai, China. Three filtrations were performed to remove solid impurities, and the filtrate as a calcium source ($CaCl_2$ solution) was reserved. The purity of compressed carbon dioxide (CO_2, 99.99%) was provided by Xi'an Beifu Gas Equipment Co., Ltd., Xi'an, China. The calcium chloride ($CaCl_2$), ammonium hydroxide (NH_4OH), sodium hydroxide ($NaOH$) and potassium hydroxide (KOH) was obtained from Sichuan Xilong Science Co., Ltd., Chengdu, China. Tianjing Damao Chemical Reagent Factory, Tianjing, China and used without further distillation.

2.2. Synthesis of Calcium Carbonate

The synthesis of calcium carbonate occurred at atmospheric temperature and without pressure in a 250 mL three flask with a gas pass into the pipe, a pH electrode and a mechanical stirrer. At the beginning of the reaction, a certain volume of 180 mL solution containing a certain concentration of $CaCl_2$ and $NH_4OH/NaOH/KOH$ mixing solution was injected into a 250 mL three flask ahead of time with constant mechanical stirring. Then, when pH monitoring equipment was placed, the gas valve was opened and 99.99% CO_2 was injected into the mixing solution. The CO_2 flow rate and stirrer speed were controlled to set experimental conditions. The precipitation of $CaCO_3$ was finished when the reaction system reached a pH value of 7 or the reaction time was reached 60 min. All the experiments in the article ended the reaction according to this condition. When the reaction was over, all produced $CaCO_3$ precipitates were filtered, washed with distilled water several times and dried at 105 °C for 6 h for subsequent detection and analysis.

2.3. Characterization

X-ray powder diffraction (XRD). The obtained particle crystalline phases were characterized using X-ray diffraction (XRD, PANalytical Empyrean, Malvern Panalytical, Malvern, GB). During the analysis, a Cu Kα source was used in the 2θ range of 20° to 60°, and a step size of 0.02° and a dwell time of 0.05 s were used. According to the obtained peak intensity of XRD, the content of the vaterite crystal phase of the obtained $CaCO_3$ product is calculated using Equation (1) as follows [40]:

$$f_V = 7.691I_{110V}/(7.691I_{110V} + I_{104C}) \tag{1}$$

The I_C and I_V are the intensity of calcite and vaterite, respectively. The three suffixes are the Miller indices of each phase, and f_V is the content of vaterite in the precipitate.

Fourier Transform Infrared spectroscopy (FTIR). Fourier transmission infrared spectroscopy (FTIR, Nicolet 6700) was performed on uniaxially pressed powder particles blended with KBr. FTIR analysis was performed in the 4000–400 cm^{-1} range with a resolution of 4 cm^{-1} and 32 repetitions of spectral scans per pattern.

Scanning Electron Spectroscopy (SEM). The particle shape and size were analyzed using scanning electron microscopy (SEM, ZEISS Sigma, Cambridge, UK, 300). The powder samples for SEM were shown and observed at a working distance of 3.5 mm and a stimulation voltage of 0.7 kV.

Dynamic light scattering (DLS). Using the dynamic light scattering method, the obtained $CaCO_3$ particle, D50 size and particle size distribution were researched by Laser particle size analysis (OMCC, SCF-106A).

2.4. Experimental Scheme

To identify the influence of chosen variables on the percentage content of vaterite in the obtained sedimentary $CaCO_3$ particles, the response surface methodology (RSM) as a research method technology was implemented. A three-level three-factor Box–Behnken was constructed using Minitab 19 statistical software (Minitab Inc., State College, PA, USA).

For the separate variables, initial $CaCl_2$ concentration (A), gas flow rate (B) and stirring speed (C) were chosen. Each parameter was tested on three levels: low (−1), high (+1) and midpoint (0). Table 1 summarizes the level values for the different variables. Table 2 showed the Box–Behnken matrix of reaction conditions.

Table 1. Range and levels of parameters in Box–Behnken experimental design.

Factors	Parameters	Coded Levels		
		−1	**0**	**+1**
A	Initial $CaCl_2$ concentration (mol·L^{-1})	0.3	0.6	0.9
B	Gas flow rate (mL·min^{-1})	300	600	900
C	Stirring speed (rpm)	300	600	900

Table 2. Box–Behnken matrix.

Experiment Number	A	B	C	Initial $CaCl_2$ Concentration (mol·L^{-1})	Gas Flow Rate (mL·min^{-1})	Stirring Speed (rpm)
1	−1	−1	0	0.3	300	600
2	+1	−1	0	0.9	300	600
3	−1	+1	0	0.3	900	600
4	+1	+1	0	0.6	600	600
5	−1	0	−1	0.3	600	300
6	+1	0	−1	0.9	600	300
7	−1	0	+1	0.3	600	900
8	+1	0	+1	0.9	600	900
9	0	−1	−1	0.6	300	300
10	0	+1	−1	0.6	900	300
11	0	−1	+1	0.6	300	900
12	0	+1	+1	0.6	900	900
13	0	0	0	0.6	600	600
14	0	0	0	0.6	600	600
15	0	0	0	0.6	600	600

3. Results and Discussion

3.1. Reaction Systems on the Carbonation Ratio and Crystal Phase Composition

Figure 1 shows XRD patterns of $CaCO_3$ formed at the various $CaCl_2$-CO_2-MOH-H_2O reaction systems by the 0.30–0.90 mol/L range of initial $CaCl_2$ concentration. Figure 1 shows the strongest (hkl) peak detected is characterized at 2θ values 23.1°, 29.4°, 36.0°, 39.4°, 43.2°, 47.5° and 48.5° corresponding to (012), (104), (110), (113), (202), (018), (116), (122), (214) and (300), and several calcite crystal faces. The X-ray diffraction pattern with peaks at 2θ values of 24.9°, 27.1°, 32.8°, 43.8°, 50.1° and 55.6° corresponds to the (100), (101), (102), (110), (104) and (202) indexes, showing that the composition of the $CaCO_3$ microspheres is in the vaterite phase. The X-ray diffraction pattern with peaks at 2θ values of 28.3° corresponds to the (103) indexes, showing that the composition of the products contains fairchildite.

As shown in Figure 1a, a mixed phase of calcite and vaterite was produced in the initial $CaCl_2$ concentration range of 0.30–0.90 mol/L, with vaterite as the main component in the $CaCl_2$-CO_2-NH_3·H_2O-H_2O reaction system. The XRD pattern in Figure 1b shows that the calcite was obtained in the 0.30 and 0.60 mol/L initial $CaCl_2$ concentration. Figure 1b shows the mixture of two crystalline phases of calcite and a small amount of vaterite were obtained in the $CaCl_2$-CO_2-NaOH-H_2O system. It can be found in Figure 1c that calcite and a small amount of fairchildite were obtained in the $CaCl_2$-CO_2-KOH-H_2O reaction systems. According to the analysis in Figure 1, it can be seen that a mixture of mainly vaterite and a small amount of calcite can be obtained in the $CaCl_2$-CO_2-NH_3·H_2O-H_2O system, while a small amount of vaterite and mainly calcite was obtained in the $CaCl_2$-CO_2-NaOH-H_2O system. However, a single calcite crystal was obtained in the $CaCl_2$-CO_2-KOH-H_2O system.
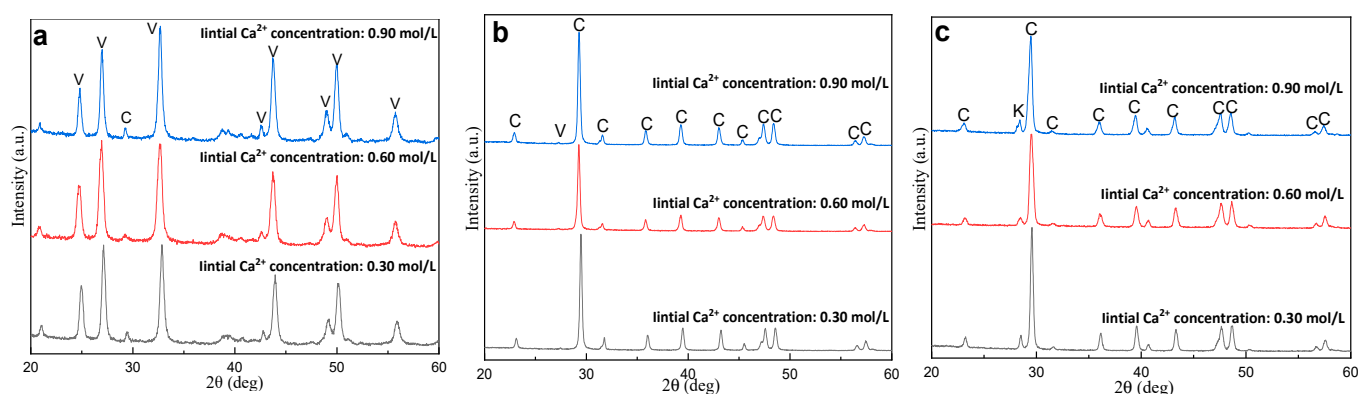
Figure 1. XRD patterns of CaCO$_3$ formed at various reaction systems. (**a**) NH$_3$·H$_2$O; (**b**) NaOH; (**c**) KOH (C$_{MOH}$:C$_{Ca^{2+}}$ = 2:1, T = 25 °C, V$_{CO_2}$ = 300 mL/min, Stirring speed = 900 rpm/min; V vaterite; C: calcite; K: fairchildite).

Table 3 shows the carbonation ratio in different CaCl$_2$-CO$_2$-OH-H$_2$O reaction systems with initial CaCl$_2$ concentrations of 0.30–0.90 mol/L. The carbonation ratio of Ca^{2+} increased with the increase in the initial CaCl$_2$ concentration. When the initial calcium concentration of reaction system is 0.90 mol/L, then the obtained calcium carbonate yield is 79.94% in the ammonia system, while in the sodium hydroxide and potassium hydroxide system, it is 99.25% and 95.60%, respectively.

Table 3. Effect of initial MOH concentration and reaction systems on the carbonation ratio (C$_{MOH}$:C$_{Ca^{2+}}$ = 2:1, T = 25 °C, V$_{CO_2}$ = 300 mL/min, r = 900 rpm).

Reaction System	Carbonation Ratio (%)	Initial Ca^{2+} Concentration (mol/L)		
		0.30	0.60	0.90
NH$_3$·H$_2$O		70.48	71.80	79.94
NaOH		82.98	92.85	99.25
KOH		91.02	95.14	95.60

The combined analysis of Figure 1 and Table 3 shows that the CaCl$_2$-CO$_2$-NH$_3$·H$_2$O-H$_2$O reaction system is conducive to formation vaterite, but the carbonation ratio is low compared the CaCl$_2$-CO$_2$-NaOH-H$_2$O and CaCl$_2$-CO$_2$-KOH-H$_2$O reaction systems.

3.2. Effect of Reaction Parameter on Crystal Phase Use Different Calcium Sources
3.2.1. Effect of Initial CaCl$_2$ Concentration on Crystal Phase

Figures 2a and 3a shows the characteristic X-ray diffraction peaks of CaCO$_3$ particles obtained at steamed ammonia liquid waste and the analysis of pure calcium chloride with different initial CaCl$_2$ concentrations. Figure 2a shows that use steamed ammonia liquid waste is a source of calcium, and the XRD results confirm that the obtained CaCO$_3$ particles are a mixture of vaterite and calcite polymorphs caused by the initial CaCl$_2$ concentration from 0.15 to 0.60 mol/L, but the calcite peak disappears when the original CaCl$_2$ concentration increases to 0.75 mol/L and 0.90 mol/L. Figure 2b shows that when the initial CaCl$_2$ concentration increased from 0.15 mol/L to 0.90 mol/L, the content of vaterite increased from 85.16% to 99.36%. It can be concluded from Figure 2 that a single-phase vaterite CaCO$_3$ particle was obtained when the initial CaCl$_2$ is increased to 0.90 mol/L. As can be seen from Figure 3a, a mixture of calcite and vaterite CaCO$_3$ was obtained when the initial CaCl$_2$ concentration was from 0.15 mol/L to 0.90 mol/L by using analyzed pure calcium chloride as the calcium source. Figure 3b shows that the content of vaterite increased from 80.28% to 96.51% with the increase in initial CaCl$_2$ from 0.15 mol/L to

0.90 mol/L. As can be seen in Figure 3, a vaterite $CaCO_3$ content of 96.51% was obtained when the initial $CaCl_2$ concentration was 0.90 mol/L.
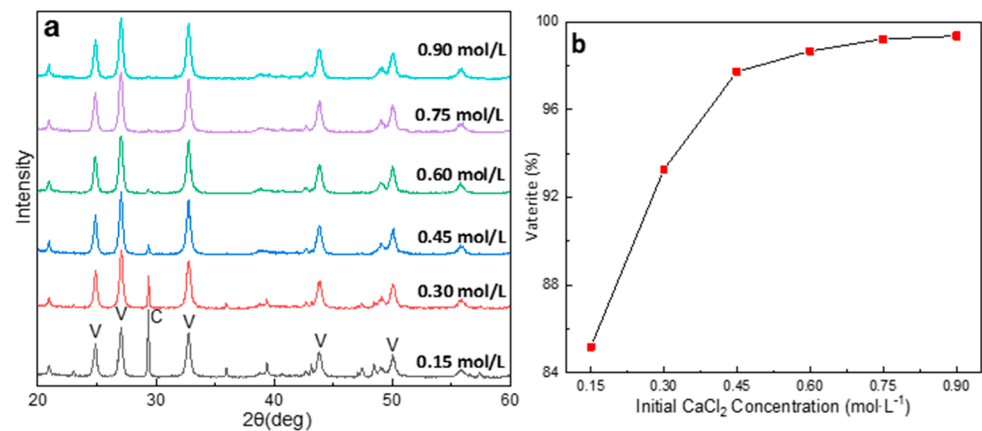

Figure 2. (**a**) XRD patterns of $CaCO_3$ phase and vaterite content with diverse. (**b**) Initial $CaCl_2$ concentration using steamed ammonia liquid waste as the calcium source. (Stirring speed = 900 rpm; CO_2 flow rate: 300 mL/min; C: calcite, V: vaterite).
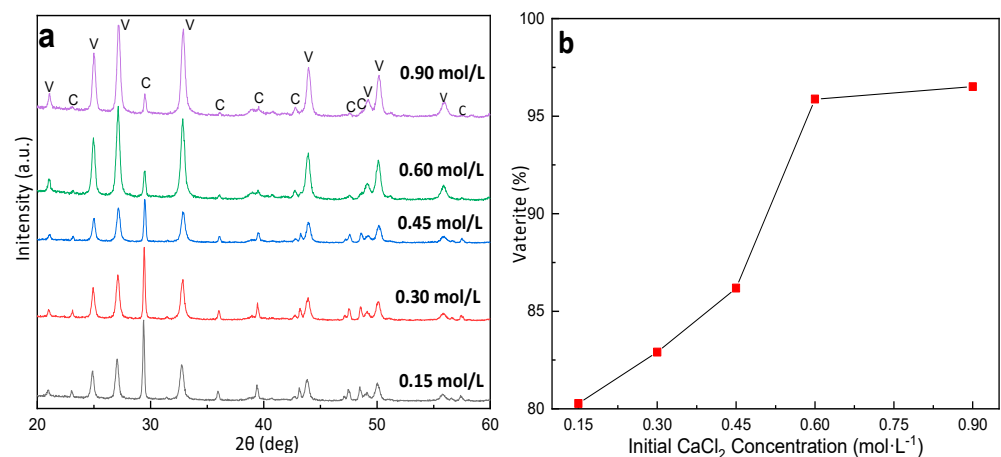

Figure 3. (**a**) XRD patterns of $CaCO_3$ phase and vaterite content with diverse. (**b**) Initial $CaCl_2$ concentrations use analysis of pure calcium chloride as calcium sources. (Stirring speed = 900 rpm; CO_2 flow rate: 300 mL/min; C: calcite, V: vaterite).

Figures 2a and 3a XRD can show that the high content vaterite particles were obtained in the higher initial $CaCl_2$ solution concentration for all conditions. This result also indicates that a higher initial $CaCl_2$ concentration is beneficial to the formation and stable existence of vaterite, which is consistent with the research results of Mohammad Hossein Azarian et al. [41]. Based on Ostwald's step rule [42], the difference in the interfacial energy between polymorphs dominates, and the metastable state tends to deposit at high supersaturation. Therefore, vaterite particles with a single crystal phase are formed under the high initial $CaCl_2$ concentration condition. According to the analysis in Figures 2 and 3, the high vaterite $CaCO_3$ was obtained by use steamed ammonia liquid waste as the calcium source as opposed to the analyzed pure calcium chloride. It can be concluded that steamed ammonia liquid waste is more conducive to the formation of vaterite products than analyzed pure calcium chloride.

Figure 4 shows the SEM pictures of the synthesized samples using various initial $CaCl_2$ concentrations. It can be seen in Figure 4a,d that when the original $CaCl_2$ concentration is 0.15 mol/L, the obtained $CaCO_3$ exhibits spherical vaterite particles and cubic calcite aggregates; these results agree with the XRD pattern (Figure 4a). The enlarged SEM images

of Figure 4d reveals that the spherical vaterite was covered with cubic calcite shapes due to the coacervation of small particles. Figure 4b,e shows the prepared $CaCO_3$ particles presenting an unparalleled morphology of rhombohedral calcite and spherical vaterite chimera. As shown in Figure 4b,e (indicated by the red circle), there are some abnormal gaps similar to the nanoparticles of vaterite on the surface of the cubic calcite. As illustrated in Figure 4c, the number of spherical particle crystal aggregates became small with the increasing initial $CaCl_2$ concentration. It can be seen in Figure 4g,h,j,k that the obtained product contains only cubic calcite particles. Still, the degree of obtained particle reunion is similar to that seen in Figure 4c,f, and this result is consistent with the particle size test. In the sample morphology in Figure 4i,l, the cubic calcite particles disappeared and only spherical vaterite particles were present when the original $CaCl_2$ concentration increased to 0.90 mol/L.
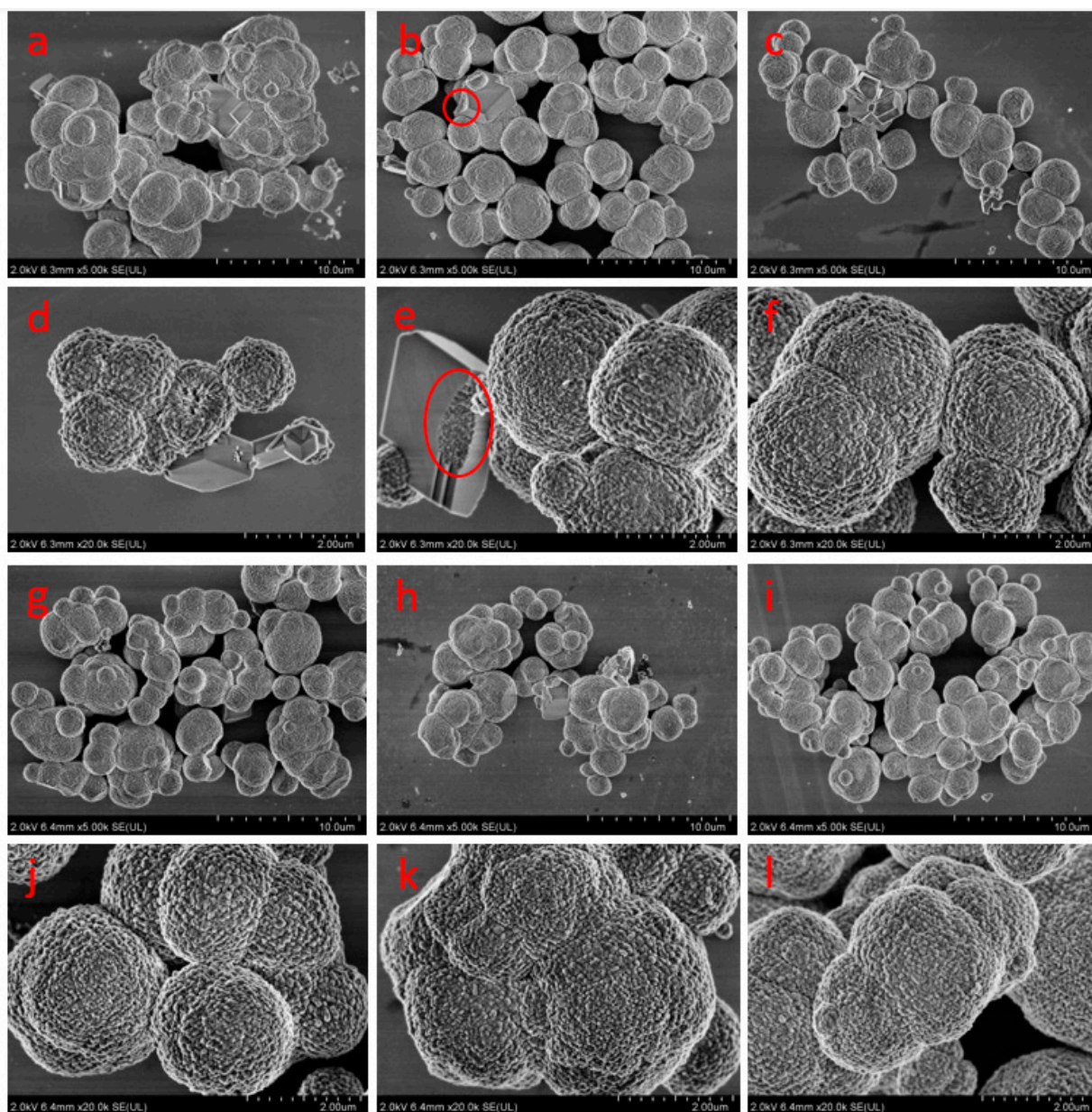

Figure 4. Morphologies of vaterite $CaCO_3$ obtained with different initial $CaCl_2$ concentrations using steamed ammonia liquid waste. ((**a**,**d**) 0.15 mol/L; (**b**,**e**) 0.30 mol/L; (**c**,**f**) 0.45 mol/L; (**g**,**j**) 0.60 mol/L; (**h**,**k**) 0.75 mol/L; (**i**,**l**) 0.90 mol/L; stirring speed = 900 rpm; CO_2 flow rate: 300 mL/min).

3.2.2. Effect of Stirring Speed and CO_2 Flow Rate on Crystal Phase Use Different Calcium Sources

The above results indicate that only vaterite particles were obtained in the high $CaCl_2$ concentration so that the initial reaction concentration of $CaCl_2$ all set were 0.30 mol/L in order to research stirring speed and CO_2 flow rate on crystal phase of particles. The effect of stirring speed and CO_2 flow rate on the phase composition of used steamed ammonia liquid waste as the calcium source was characterized via XRD, as shown in Figure 5. A mixture of vaterite and calcite was obtained with varying stirring speeds and CO_2 flow rate when using steamed ammonia liquid waste, as is shown in Figure 5. Figure 5a shows that the vaterite peak (110), (112), and (114) becomes stronger with the increasing CO_2 flow rate and that the calcite (104) peak decreases with the increasing CO_2 flow rate at 300 rpm stirring speed. Figure 5b shows that the intensity of the (110), (112) and (114) peaks for vaterite slightly decreases with the increasing CO_2 flow rate. Figure 5c shows that the intensity of the (110), (112) and (114) peaks of vaterite and the intensity peak of the (104) peak for calcite are almost unchanged. It can be seen in Figure 5 that the peak intensity of calcite (104) crystal decreases and that the peak intensity of vaterite increases slightly with the increase in stirring speed at the same CO_2 flow rate.
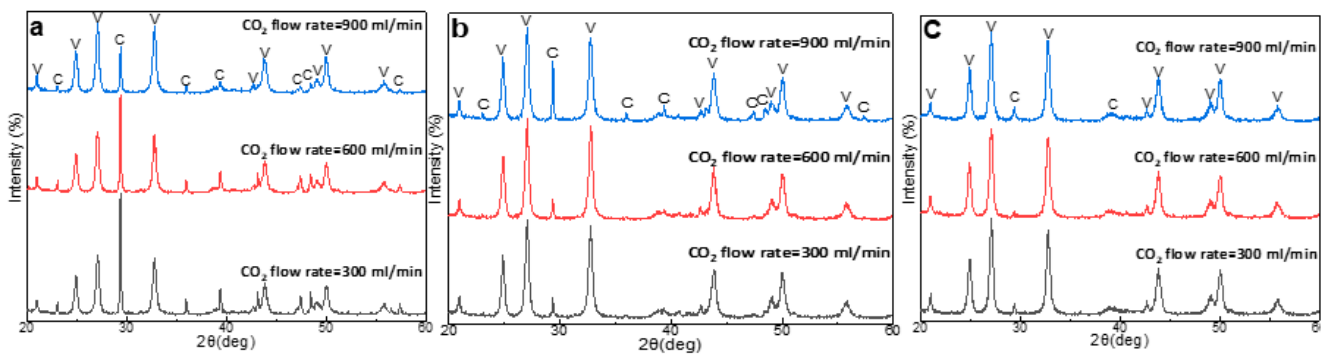

Figure 5. XRD patterns of $CaCO_3$ crystal obtained with diverse stirring speed and CO_2 flow rate when using steamed ammonia liquid waste as the calcium source. Stirring speed: (**a**) 300 rpm; (**b**) 900 rpm/min and (**c**) 900 rpm/min. (Initial $CaCl_2$ concentration = 0.30 mol/L; C: calcite, V: vaterite).

Table 4 shows that the content of vaterite increases from 79.03% to 91.94% with the increase in CO_2 flow rate under a stirring speed of 300 rpm. With a stirring speed of 600 rpm, the content of aragonite decreases from 97.15% to 92.15% with the increase in CO_2 flow rate. Under the reaction condition of 900 rpm, the content of vaterite decreases from 98.18% to 97.70% with the increase in CO_2 flow rate. It can also be seen in Table 4 that the content of vaterite increases continuously under the same CO_2 flow rate with the increase in stirring speed. It can be seen from the comprehensive analysis in Table 4 and Figure 6 that the stirring speed and CO_2 flow rate have a great synergistic effect on the content of vaterite.

Table 4. Content of vaterite obtained with different stirring speed and CO_2 flow rate using steamed ammonia liquid waste as the calcium source.

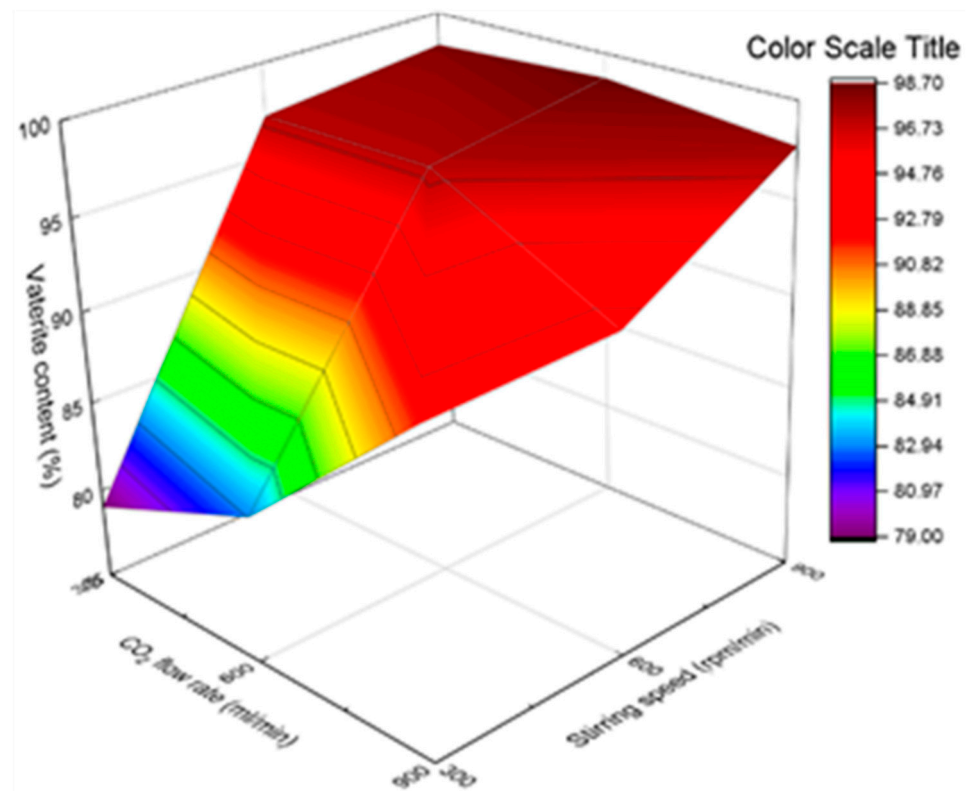| Stirring Speed (r/min)	Content (%)	CO₂ Flow Rate (mL/min)		
		300	600	900
300		79.03	82.97	91.94
600		97.15	97.19	92.15
900		98.18	98.69	97.70

Figure 6. Three-dimensional response surface content of vaterite obtained under different stirring speed and CO_2 flow rate using steamed ammonia liquid waste as the calcium source.

The effect of stirring speed and CO_2 flow rate on the phase composition, using the analysis of the pure calcium chloride, was characterized via XRD and are shown in Figure 7a,b. A mixture of vaterite and calcite was obtained with diverse stirring speed and CO_2 flow rate using the analysis of the pure calcium chloride, as shown in Figure 7. Figure 7a indicates that the vaterite peak (110), (112) and (114) becomes stronger with the increasing stirring speed and that the calcite (104) content decreases with the increasing stirring speed. Figure 7b indicates that the vaterite peak (110), (112) and (114) becomes weaker with CO_2 flow rate and that the calcite (104) peak increases sharply with CO_2 flow rate. As can be seen from Figure 7c, the content of vaterite increases from 90.21% to 94.54% when the stirring speed increases from 200 rpm to 1200 rpm. And the content of vaterite decreased from 87.05% to 42.73% with the increase in CO_2 flow rate from 500 mL/min to 1500 mL/min.
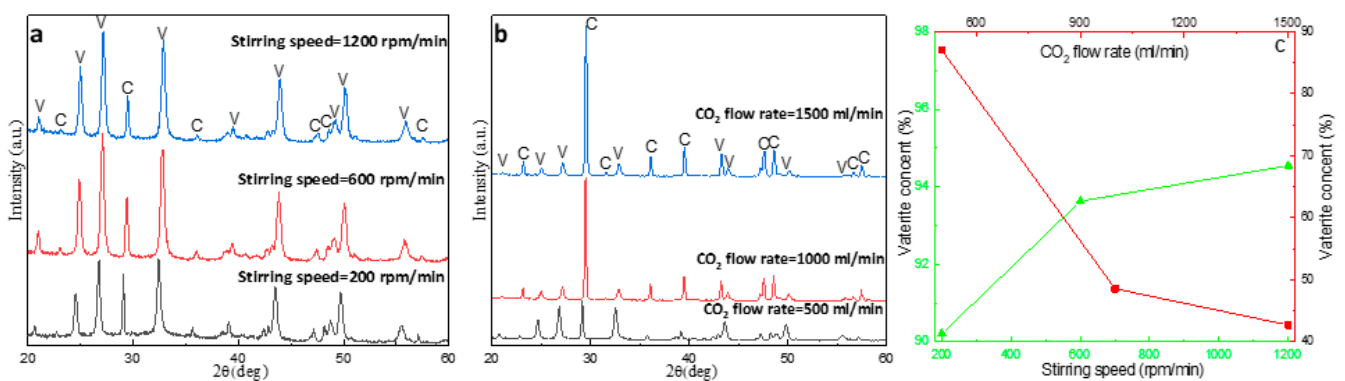

Figure 7. (**a**,**b**) XRD patterns of $CaCO_3$ crystal. (**c**) Vaterite content with varying stirring speed and CO_2 flow rate obtained using the analysis of pure calcium chloride as the calcium source; ((**a**): CO_2 flow rate = 300 mL/min; (**b**): Stirring speed = 900 rpm; Initial $CaCl_2$ concentration = 0.30 mol/L; C: calcite, V: vaterite).

According to Figures 5–7 and the comprehensive analysis, the content of vaterite increases with the increase in stirring speed when pure calcium chloride and steamed ammonia liquid waste are used as the calcium sources, respectively. The content of vaterite decreases with the increase in the CO_2 flow rate, as can be seen in Figure 5c and Table 2. It shows that the reaction conditions have the same effect on the content of vaterite when pure calcium chloride and steamed ammonia liquid waste are used as calcium sources, respectively. However, the content of vaterite caused by using steamed ammonia liquid waste as the calcium source is significantly higher than by using pure calcium chloride as the calcium source under the same conditions. It can be concluded that the special properties of the steamed ammonia liquid waste are conducive to the formation of vaterite.

3.3. Optimization of Preparation Single Vaterite by Using Steamed Ammonia Liquid Waste

In order to achieve the purpose of the preparation of single-phase vaterite $CaCO_3$ by the carbonization of steamed ammonia liquid waste, and based on the above finding that high concentration was conducive to the formation of vaterite, the initial concentration of steamed ammonia liquid waste was set at 0.60 mol/L, and the effects of stirring speed and CO_2 flow rate on the preparation of single-phase vaterite and its morphology and particle size were systematically studied.

3.3.1. Effect of $NH_3 \cdot H_2O$ Concentration on Carbonation Ratio and Crystal Phase

Figure 8a shows the carbonation ratio at an initial Ca^{2+} concentration of 0.60 mol/L under different $NH_3 \cdot H_2O$ concentrations. The carbonation ratio of Ca^{2+} increased as the $NH_3 \cdot H_2O$ concentration increased. A carbonation ratio of 96.03% was achieved under 1.8 mol/L $NH_3 \cdot H_2O$. And the carbonation ratio increased marginally as the $NH_3 \cdot H_2O$ concentration increased from 1.2 mol/L to 1.8 mol/L. AS the ammonium concentration further increased to 2.1 mol/L and 2.4 mol/L, the carbonization rate of calcium ion did not increase, but rather slightly decreased. In the ammonia system, the carbonization rate of calcium ions did not reach 100%, which is consistent with other studies [43]. Due to the volatilization of $NH_3 \cdot H_2O$ and the CO_2 absorption ratio of $NH_3 \cdot H_2O$ being less than 100%, excessive $NH_3 \cdot H_2O$ was needed in the actual experiment. With the increase in $NH_3 \cdot H_2O$ concentration, the alkalinity of the solution increased, the CO_2 absorption efficiency increased, and the concentration of CO_3^{2-} in the solution increased, thus promoting the reaction of CO_3^{2-} with Ca^{2+} to generate $CaCO_3$. Figure 8b shows the XRD patterns of $CaCO_3$ at an initial Ca^{2+} concentration of 0.60 mol/L under different $NH_3 \cdot H_2O$ concentrations. It can be seen from Figure 8 that the particles obtained under each $C_{NH_3 \cdot H_2O}/C_{Ca^{2+}}$ ratio is a mixture of calcite and vaterite, but the products are mainly composed of vaterite and only contain a very small amount of calcite.
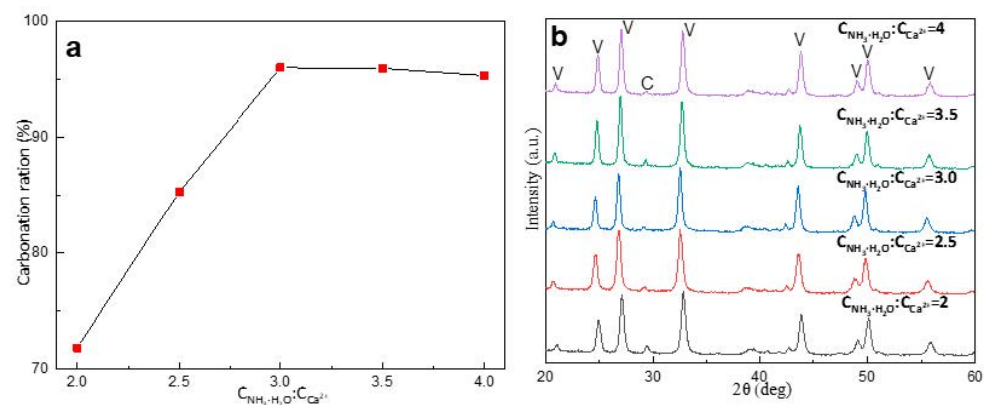

Figure 8. Effect of $NH_3 \cdot H_2O$ concentration on (**a**) the carbonation ratio and (**b**) the XRD patterns of $CaCO_3$. (V: vaterite; C: calcite; $C_{Ca^{2+}}$ = 0.60 mol/L; T = 25 °C; V_{CO_2} = 300 mL/min; stirring speed = 900 rpm).

3.3.2. Effect of Stirring Speed and CO_2 Flow Rate on Vaterite Formation

(1) Crystal Structure

The XRD patterns and FTIR spectra of the $CaCO_3$ particles were prepared at 200, 400, 600, 800, 1000 and 1200 rpm by mechanical stirring, as illustrated in Figure 9. The XRD patterns in Figure 9a indicate that the constituent of $CaCO_3$ is a single phase of vaterite produced by mechanical stirring at stirring speeds of 200, 400, 600 and 800 rpm. It can be seen from Figure 9a that a weaker peak of calcite (104) exists at the mechanical stirring speed of 1000 and 1200 rpm, which indicates that the calcite and $CaCO_3$ is inevitably contained when prepared under high-speed stirring conditions. Figure 8b shows that the phase of the product was dependent on the various mechanical stirring speeds based on the FTIR spectrum, while the FTIR further confirms the XRD results. The absorption bands of $CaCO_3$ can be divided into four units in the infrared wavelength range in relation to the C–O bond vibrations at 1087 cm^{-1}, 744 cm^{-1}, and 711 cm^{-1}. The vibrational bands at 745 cm^{-1} and 1087 cm^{-1} can be due to the ν_4 and ν_2, ν_1 patterns of CO_3^{2-} in vaterite. The characteristic peaks at 875 cm^{-1} and 711 cm^{-1} are appointed to the flexing oscillation of the C–O combination of the calcite polymorph. From the FTIR issues in Figure 9b, it can be inferred that the procured product is a pure vaterite phase prepared at 200–800 rpm by mechanical stirring. When the mechanical stirring speed reaches 1000 and 1200 rpm, which is the fingerprint ν_4 morphing band of CO_3^{2-} in calcite mode, issues arise in the emergence of a new assimilation weak peak located at 711 cm^{-1}, indicating that the sample contains a little calcite phase $CaCO_3$. Together with Figure 9, XRD pattern and FTIR spectrum, it can be concluded that the obtained particles are single vaterite $CaCO_3$ caused by an mechanical stirring speed in the range of 200–800 rpm. Figure 9 shows that the products obtained at different stirring speeds are almost a single vaterite calcium carbonate phase.
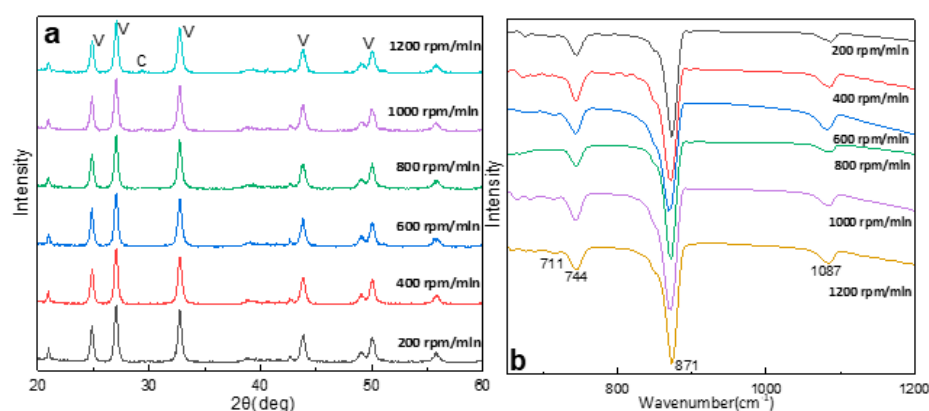

Figure 9. (**a**) XRD patterns and (**b**) FTIR spectra of $CaCO_3$ crystal prepared with different mechanical stirring speeds. (Initial $CaCl_2$ concentration = 0.60 mol/L; CO_2 flow rate: 300 mL/min; C: calcite; V: vaterite).

Figure 10 displays the XRD patterns and FTIR spectra of the crystalline polymorphs of $CaCO_3$ particles obtained at various CO_2 flow rates. As shown in Figure 10a, the predominant crystalline phase is vaterite and contains weak calcite (104), which were obtained under a CO_2 flow rate of 200 mL/min. However, the obtained particles only contain the vaterite phase when the CO_2 flow rate ranged from 400 to 1200 mL/min. The FTIR spectra of the $CaCO_3$ crystals procured in the range of 200–1200 mL/min are shown in Figure 10b, further indicating that the sample is a single vaterite phase $CaCO_3$ via the FTIR two characteristic peaks of vaterite centered at 744 cm^{-1} and 871 cm^{-1}. Figure 10 and the XRD and FTIR results indicate that the single vaterite was obtained when the CO_2 flow rate increased from 200 to 400 mL/min and remained about the same when the CO_2 flow rate increased to 1200 mL/min.
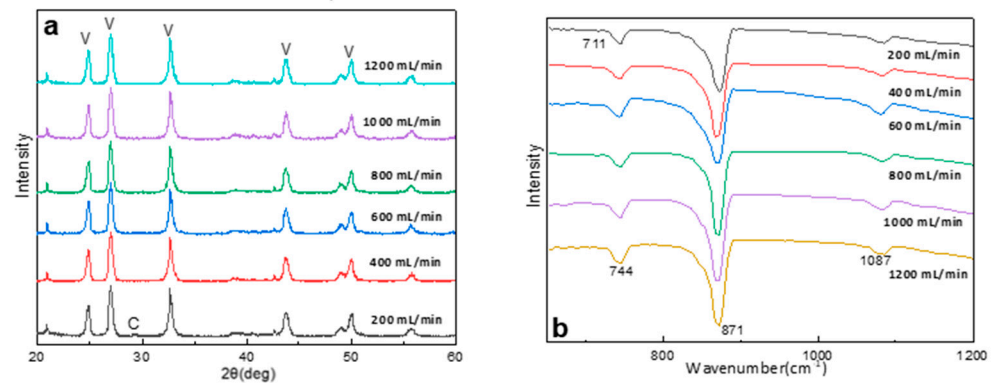
Figure 10. (**a**) XRD patterns and (**b**) FTIR spectra of $CaCO_3$ crystal obtained with different CO_2 flow rates. (Initial $CaCl_2$ concentration = 0.60 mol/L; stirring speed = 900 rpm; C: calcite; V: vaterite).

(2) Particle size

Figure 11a indicates the influence of stirring speed on the particle size distribution of the vaterite synthesized by a mechanical stirring method. Based on the LPSA images in Figure 11a it can be found that the stirring speed had a great influence on the particle size and distribution of the prepared vaterite. Figure 11a shows that the vaterite particle size D_{50} decreased from 11.10 to 8.89 μm as the stirring speed was increased from 200 to 600 rpm. When the stirring speeds were further increased to 1000 and 1200 rpm, the D_{50} particle size of samples increased to 10.92 and 10.94 μm, respectively.
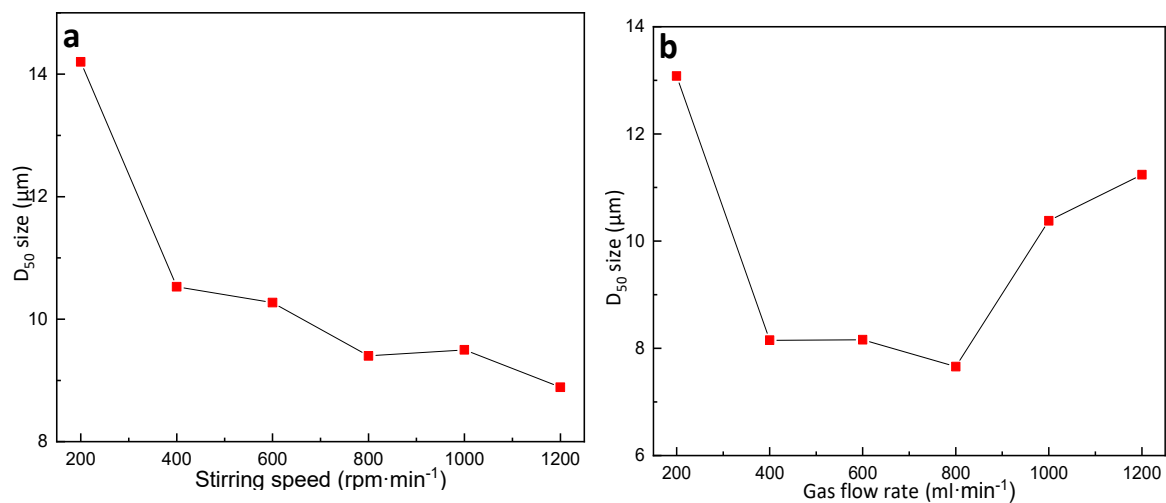

Figure 11. The particle D_{50} size diameter: (**a**) stirring speed; (**b**) CO_2 flow rate. (Initial $CaCl_2$ concentration = 0.60 mol/L; stirring speed = 900 rpm; CO_2 flow rate: 300 mL/min).

Figure 11b shows the LPSA particle size of the examples prepared at different CO_2 flow rates. Figure 11b shows that the synthetic vaterite particle size D_{50} decreased from 13.08 to 7.66 μm as the CO_2 flow rate increased from 200 to 800 mL/min. However, the particle size of the vaterite products increased sharply with the further increase in CO_2 flow rate. The D_{50} particle size of samples increased by 11.24 μm when the CO_2 flow rate was further increased to 1200 mL/min.

(3) Particle morphology

As shown in Figure 12, SEM indicated a visible exchange in the morphology and polymorphism of the $CaCO_3$ crystals with the 200, 600 and 1200 rpm stirring speed. Figure 12 indicates that the abnormal nanoscale spherical vaterite begins to aggregate, and large spherical aggregates were obtained with stirring speeds of 200, 600 and 1200 rpm.

Figure 12b,c shows that when the stirring speed was increased to 600 rpm, the sample contained almost completely spherical particle agglomerates. Still, the particles exhibited a considerably smaller particle size and a lower degree of agglomeration than the other samples (Figure 12a,d). Figure 12c,f shows that the vaterite samples' morphology was similar to that prepared at the same stirring speed of 600 rpm. By combining SEM and XRD, a feasible interpretation is that the stirring speed can change the phase formation and grain aggregation of vaterite particles. By combining SEM and LPSA, it can be found that the obtained vaterite particle size decreases continuously with the increase in stirring speed.
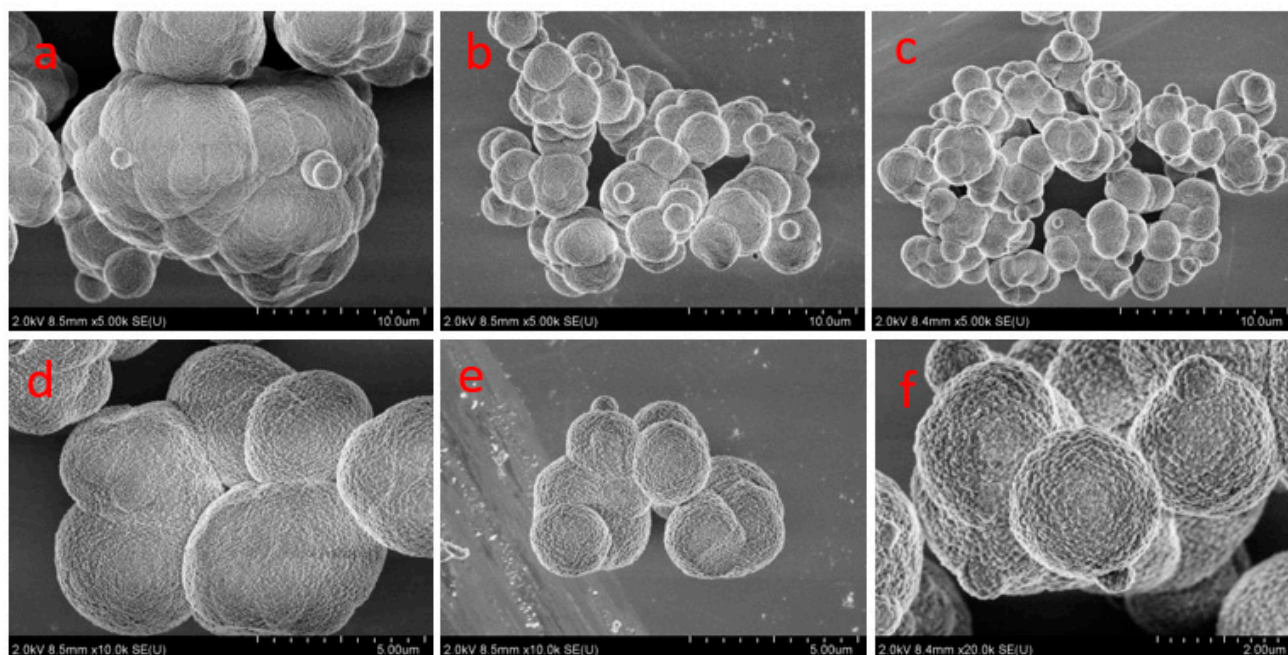

Figure 12. Morphologies of vaterite $CaCO_3$ crystal obtained with different stirring speeds. ((**a**,**d**): 200 rpm; (**b**,**e**): 600 rpm; (**c**,**f**): 1200 rpm; initial $CaCl_2$ concentration = 0.60 mol/L; CO_2 flow rate: 300 mL/min).

SEM characterized the shapes of the as-prepared examples with mechanical stirring modes at different CO_2 flow rates. The corresponding results are presented in Figure 13. It can be observed from Figure 13 that at the CO_2 flow rate of 200, 600 and 1200 mL/min, all the samples are aggregate spherical vaterite $CaCO_3$ and that the morphology of vaterite particles shows no significant changes with the increase in CO_2 flow rate. From Figure 13a,b,d,e, can be seen that the amount of vaterite and degree of aggregation decreased, leading to the particle size of vaterite products decreasing when the CO_2 flow rate increased from 200 to 600 mL/min. Pure spherical vaterite was obtained with a CO_2 flow rate in the tested concentration range. These results suggest that it is beneficial to obtain single-phase spherical vaterite products using steamed ammonia liquid waste as raw material at different CO_2 flow rates.

To further prove that steamed ammonia liquid waste liquid is extremely beneficial to obtaining single-phase vaterite, the Box–Behnken experimental design was used to design the experimental scheme. The influences of three technological parameters, including initial $CaCl_2$ concentration, stirring speed, and CO_2 flow rate on the content of vaterite, were studied. The results are shown in Table 5.
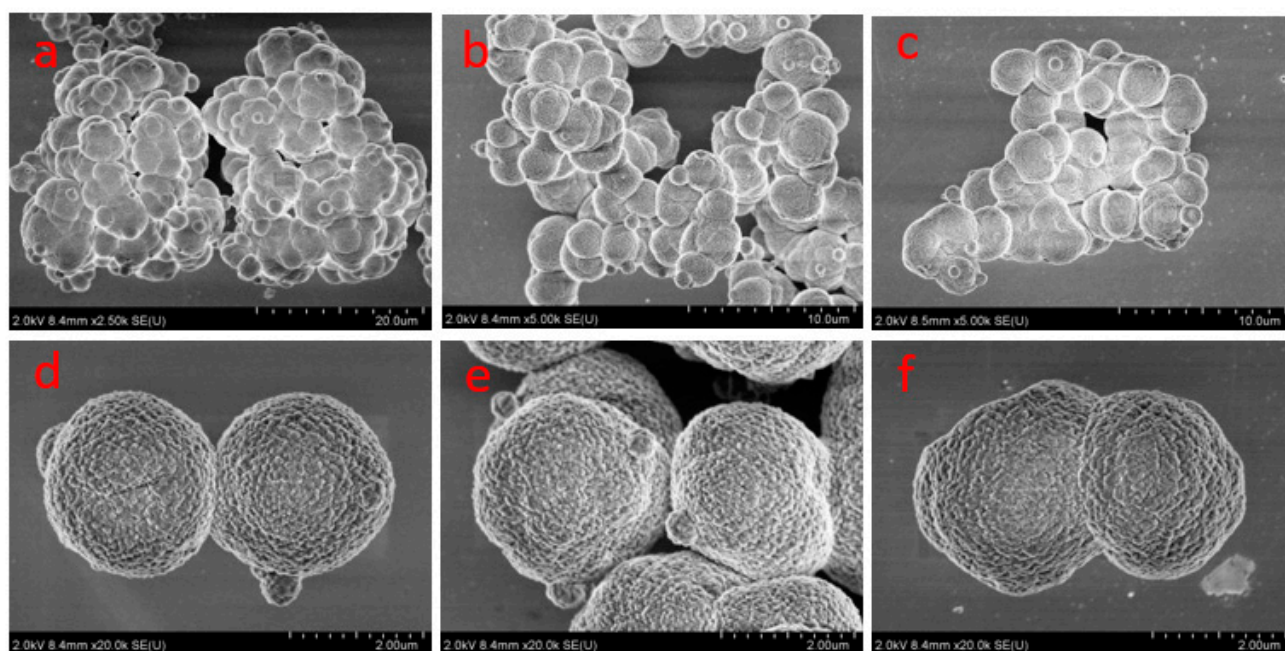
Figure 13. Morphologies of vaterite $CaCO_3$ crystal obtained with different CO_2 flow rates. ((**a**,**d**): 200 mL/min; (**b**,**e**): 600 mL/min; (**c**,**f**): 1200 mL/min; initial $CaCl_2$ concentration = 0.60 mol/L; stirring speed = 900 rpmp).

Table 5. The percentage vaterite content obtained under different preparation conditions.

Samples	1	2	3	4	5	6	7	8
Content (%)	99.13	99.46	99.38	99.03	99.01	99.05	99.47	99.41
Samples	9	10	11	12	13	14	15	
Content (%)	98.98	99.47	99.44	98.87	99.20	99.38	99.51	

It can be seen from the Box–Behnken results in Table 5 that the obtained samples of $CaCO_3$ had a percentage vaterite content that was approaching 100%, and single-phase vaterite products could be obtained within the selected range of conditions. These results indicate that using steamed ammonia liquid waste and CO_2 as sources were good for forming single-phase vaterite particles by an indirect carbonation route.

3.4. Possible Mechanism of Steamed Ammonia Liquid Waste in the Formation of Vaterite

Our previous work [44] attributed the formation of metastable vaterite to the unique synthesis system that included steamed ammonia liquid waste. However, our previous research also indicated that single vaterite required strict reaction conditions by using steamed ammonia liquid waste and $(NH_4)CO_3$ [45]. However, it is not necessary to strictly control the technological parameters of the reaction process using steamed ammonia liquid waste via a carbonation route and prepared single-vaterite $CaCO_3$, which shows that this method is beneficial to the formation of single-phase spherical vaterite particles. In conclusion, combining steamed ammonia liquid waste and CO_2 as sources was crucial in forming single vaterite-phase $CaCO_3$.

Through the previous studies, it can be shown that the steamed ammonia liquid waste is conducive to the formation of vaterite, and that the mechanism of the steamed ammonia liquid waste properties in the crystallization behavior of vaterite and phase stability is analyzed. It is speculated that the analysis may be related to the special properties of the steamed ammonia liquid waste itself. According to the source of the steamed ammonia liquid waste, the possible impurity ions in the steamed ammonia liquid waste are tested. Table 6 lists the impurity ions in the steamed ammonia liquid waste.

Table 6. Content of main impurity ions in steamed ammonia liquid waste experimental reagent.

Ions	K^+	Na^+	Mg^{2+}	S^{2-}	Ammonia Nitrogen
Concentration (mol/L)	0.014	0.054	0.0058	0.0028	0.036

Through systematic analysis and relevant detection, it was determined that there were no other impurity ions except the related ions listed. Due to the high initial pH of the steamed ammonia liquid waste (11.17), in order to accurately understand the role of the special properties of the steamed ammonia liquid waste in the formation of vaterite, the pH of pure $CaCl_2$ solution analyzed at different concentrations was tested, and the results are shown in Figure 13.

Table 6 shows that the impurity ions in the steamed ammonia liquid waste are strong alkaline cations, namely Mg^{2+}, K^+, Na^+ and NH_4^+, and that the initial pH of the steamed ammonia liquid waste is as high as 10.53. Figure 14 shows that solid $CaCl_2$ particles are completely insoluble when 2.10 mol/L was added and that the pH of the solution does not exceed 11. It can be concluded that the presence of these ions leads to an initial pH of the steamed ammonia liquid waste as high as 10.53, and the presence of these ions can promote the saturation solubility of $CaCl_2$. It has been reported that Mg^{2+}, K^+ and Na^+ can change the nucleation and crystallization process of $CaCO_3$ [46,47]. Some studies have shown that when the initial $CaCl_2$ solution is more alkaline, the vaterite phase transition to calcite can be prevented in the reaction system, thus realizing the synthesis of vaterite products [48]. Some studies have also shown that the presence of NH_4^+ ions can provide a certain role in the stable existence of vaterite-phase $CaCO_3$ [49]. Combined with the above analysis results and related studies, it can be concluded that the special properties of steamed ammonia liquid waste have the following two roles in formation of vaterite: (1) First, the existence of Mg^{2+}, K^+ and Na^+ can change the formation of calcium carbonate so that vaterite is obtained. Second, the strong alkalinity of the initial steamed ammonia liquid waste and the presence of NH_4^+ can prevent the phase transition from vaterite to calcite.
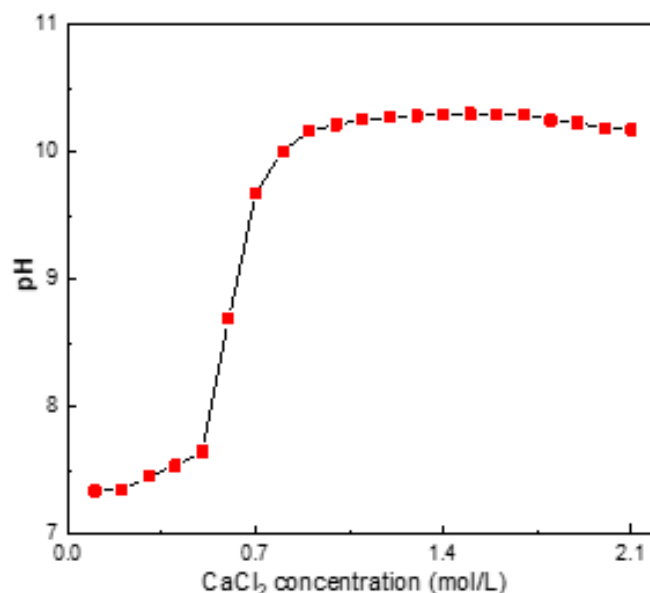
Figure 14. Relationship between pH of solution and $CaCl_2$ (analytical grade) concentration.

4. Conclusions

The aim of the study was achieving the production of vaterite by using the high-value utilization of steamed ammonia liquid waste and CO_2. Different factors influencing the formation of vaterite were investigated, and the following conclusions could be drawn:

(1) The research indicated that the $CaCl_2$-CO_2-$NH_3 \cdot H_2O$-H_2O reaction system is conducive to the formation of vaterite, but the $CaCl_2$-CO_2-$NaOH$-H_2O and $CaCl_2$-CO_2-KOH-H_2O systems are not conducive to the formation of vaterite when using steamed ammonia liquid waste as the calcium source.

(2) The content of vaterite by using steamed ammonia liquid waste as the calcium source was significantly higher than that obtained by using pure calcium chloride as the calcium source.

(3) A vaterite $CaCO_3$ content of 96.51% was obtained when the initial concentration of $CaCl_2$ was 0.90 mol/L, and the content of vaterite increased with the increase in stirring speed.

(4) The particles obtained at each $C_{NH_3 \cdot H_2O}/C_{Ca^{2+}}$ ratio is a mixture of calcite and vaterite, but the products are mainly composed of vaterite and only contain a very small amount of calcite. The obtained samples of $CaCO_3$ that have a percentage vaterite content approaching 100% as well as single-phase vaterite products can be obtained within the selected range of conditions.

(5) The research indicated that the steamed ammonia liquid waste was more conducive to the formation of vaterite products than the analyzed pure calcium chloride.

This paper provided a novel integration approach of single-phase vaterite $CaCO_3$ using steamed ammonia liquid waste through an indirect carbonation method. This research can achieved a method of energy saving and emission reduction, and the solidification of CO_2. Moreover, this work can help develop a more feasible method to realize the preparation of vaterite particles, promote the process of vaterite industrial production and expand the application scope of vaterite.

Institutional Review Board Statement: Not applicable.

Informed Consent Statement: Not applicable.

Data Availability Statement: No new data was created, or the data are not available due to privacy or ethical restrictions.

Conflicts of Interest: We declare that we have no financial and personal relationship with other people or organizations that can inappropriately influence our work.

References

1. Luo, X.; Song, X.; Cao, Y.; Song, L.; Bu, X. Investigation of calcium carbonate synthesized by steamed ammonia liquid waste without use of additives. *RSC Adv.* **2020**, *10*, 7976–7986. [CrossRef]

2. Wang, B.; Pan, Z.; Cheng, H.; Guan, Y.; Zhang, Z.; Cheng, F. CO_2 sequestration: High conversion of gypsum into $CaCO_3$ by ultrasonic carbonation. *Environ. Chem. Lett.* **2020**, *18*, 1369–1377. [CrossRef]

3. Yu, L.; Rui, L.; Dong, F. Quaternary phosphonium cationic ionic liquid/porous metal–organic framework as an efcient catalytic system for cycloaddition of carbon dioxide into cyclic carbonates. *Environ. Chem. Lett.* **2019**, *17*, 501–508. [CrossRef]

4. Lu, J.; Li, X.; Zhao, Y.; Ma, H.; Wang, L.; Wang, X.; Yu, Y.; Shen, T.; Xu, H.; Zhang, Y. CO_2 capture by ionic liquid membrane absorption for reduction of emissions of greenhouse gas. *Environ. Chem. Lett.* **2019**, *17*, 1031–1038. [CrossRef]

5. Liu, Z.; Yi, X.; Gao, F.; Xie, Z.; Han, B.; Sun, Y.; He, M.; Yang, J. Green Carbon Science: A Scientific Basis for Achieving 'Dual Carbon' Goal-Academic Summary of the 292nd "Shuang-Qing Forum". *Acta Phys. Chim. Sin.* **2022**, *38*, 2112029. [CrossRef]

6. Olabisi, L.S.; Reich, P.B.; Johnson, K.A.; Kpusciski, A.R.; Suh, S.; Wilsonr, E.J. Reducing Greenhouse Gas Emissions for Climate Stabilization: Framing Regional Options. *Environ. Sci. Technol.* **2009**, *43*, 1696–1703. [CrossRef]

7. Wang, Q.; Luo, J.; Zhong, Z.; Borgna, A. CO_2 capture by solid adsorbents and their applications: Current status and new trends. *Energy Environ. Sci.* **2011**, *4*, 42–55. [CrossRef]

8. Goeppert, A.; Czaun, M.; Prakash, G.K.S.; Olah, G.A. Air as the renewable carbon source of the future: An overview of CO_2 capture from the atmosphere. *Energy Environ. Sci.* **2012**, *5*, 7833–7853. [CrossRef]

9. North, M.; Pasqualea, R.; Young, C. Synthesis of cyclic carbonates from epoxides and CO_2. *Green Chem.* **2010**, *12*, 1514–1539. [CrossRef]

10. Shang, J.; Liu, S.; Ma, X.; Lua, L.; Deng, Y. A new route of CO_2 catalytic activation: Syntheses of N-substituted carbamates from dialkyl carbonates and polyureas. *Green Chem.* **2012**, *14*, 2899–2906. [CrossRef]

11. Han, K.; Ahn, C.; Lee, M.S.; Rhee, C.H.; Kim, J.Y.; Chun, H.D. Current status and challenges of the ammonia-based CO_2 capture technologies toward commercialization. *Int. J. Greenh. Gas Control* **2013**, *14*, 270–281. [CrossRef]

12. Kirchofer, A.; Becker, A.; Brandt, A.; Wilcox, J. CO_2 mitigation potential of mineral carbonation with industrial alkalinity sources in the united states. *Environ. Sci. Technol.* **2013**, *47*, 7548–7554. [CrossRef]

13. Lam, T.D.; Hoang, T.V.; Quang, D.T.; Kim, J.S. Effect of nanosized and surface-modified precipitated calcium carbonate on properties of CaCO3/polypropylene nanocomposites. *Mat. Sci. Eng. A* **2009**, *501*, 87–93. [CrossRef]

14. Karakaş, F.; Hassas, B.V.; Çelik, M.S. Effect of precipitated calcium carbonate additions on waterborne paints at different pigment volume concentrations. *Prog. Org. Coat.* **2015**, *83*, 64–70. [CrossRef]

15. Shen, J.; Song, Z.; Qian, X.; Yang, F. Carboxymethyl cellulose/alum modified precipitated calcium carbonate fillers: Preparation and their use in papermaking. *Carbohyd. Polym.* **2010**, *81*, 545–553. [CrossRef]

16. Said, A.; Mattila, H.-P.; Järvinen, M.; Zevenhoven, R. Production of precipitated calcium carbonate (PCC) from steelmaking slag for fixation of CO_2. *Appl. Energ.* **2013**, *112*, 765–771. [CrossRef]

17. Trushina, D.B.; Bukreeva, T.V.; Kovalchuk, M.V.; Antipina, M.N. $CaCO_3$ vaterite microparticles for biomedical and personal care applications. *Mat. Sci. Eng. C* **2014**, *45*, 644–658. [CrossRef] [PubMed]

18. Lu, J.; Cong, X.; Li, Y.; Hao, Y.; Wang, C. Scalable recycling of oyster shells into high purity calcite powders by the mechanochemical and hydrothermal treatments. *J. Clean. Prod.* **2018**, *172*, 1978–1985. [CrossRef]

19. Zhang, W.; Zhang, F.; Ma, L.; Ning, P.; Yang, J.; Wei, Y. An efficient methodology to use hydrolysate of phosphogypsum decomposition products for CO_2 mineral sequestration and calcium carbonate production. *J. Clean. Prod.* **2020**, *259*, 120826. [CrossRef]

20. Chen, Q.; Ding, W.; Sun, H.; Peng, T.; Ma, G. Utilization of Phosphogypsum to Prepare High-Purity $CaCO_3$ in the $NH_4Cl{-}NH_4OH{-}CO_2$ System. *ACS Sustai. Chem. Eng.* **2020**, *8*, 11649–11657. [CrossRef]

21. Altiner, M.; Top, S.; Kaymakoğlu, B.; Seçkin, İ.Y.; Vapur, H. Production of precipitated calcium carbonate particles from gypsum waste using venturi tubes as a carbonation zone. *J. CO2 Util.* **2019**, *29*, 117–125. [CrossRef]

22. Altiner, M. Use of Taguchi approach for synthesis of calcite particles from calcium carbide slag for CO_2 fixation by accelerated mineral carbonation. *Arab. J. Chem.* **2019**, *12*, 531–540. [CrossRef]

23. Mao, S.; Liu, Y.; Zhang, T.; Li, X. Nano-$CaCO_3$ synthesis by jet-reactor from calcium carbide slag. *Mater. Res. Express* **2020**, *7*, 115003. [CrossRef]

24. Korkut, I.; Civas, A.; Bayramoglu, M. Effects of ultrasound and process parameters on the precipitation of $CaCO_3$ polymorphs from synthetic soda ash industry liquid waste. *Chem. Eng. Process.* **2021**, *168*, 108584. [CrossRef]

25. Jeona, J.; Kim, M.-J. CO_2 storage and $CaCO_3$ production using seawater and an alkali industrial by-product. *Chem. Eng. J.* **2019**, *378*, 122180. [CrossRef]

26. Gao, C.; Dong, Y.; Zhang, H.; Zhang, J. Utilization of distiller waste and residual mother liquor to prepare precipitated calcium carbonate. *J. Clean. Prod.* **2007**, *15*, 1419–1425. [CrossRef]

27. Trypuc, M.; Bialowicz, K. CaCO3 production using liquid waste from Solvay method. *J. Clean. Prod.* **2007**, *19*, 751–756. [CrossRef]

28. Ishikawa, K.; Freitas, P.; Kishida, R.; Hayashi, K.; Tsuchiya, A. Fabrication of vaterite blocks from a calcium hydroxide compact. *Ceram. Int.* **2022**, *48*, 4153–4157. [CrossRef]

29. Liu, M.; Gadikota, G. Single-step, low temperature and integrated CO_2 capture and conversion using sodium glycinate to produce calcium carbonate. *Fuel* **2020**, *275*, 117887. [CrossRef]

30. Li, W.; Huang, Y.; Wang, T.; Fang, M.; Li, Y. Preparation of calcium carbonate nanoparticles from waste carbide slag based on CO_2 mineralization. *J. Clean. Prod.* **2022**, *363*, 132463. [CrossRef]

31. Shen, P.; Yi, J.; Zhang, Y.; Liu, S.; Xuan, D.; Lu, J.; Zhang, S.; Sun, C. Production of aragonite whiskers by carbonation of fine recycled concrete wastes: An alternative pathway for efficient CO_2 sequestration. *Renew. Sust. Energ. Rev.* **2023**, *173*, 113079. [CrossRef]

32. Kim, S.; Jeon, J.; Kim, M. Vaterite production and particle size and shape control using seawater as an indirect carbonation solvent. *J. Environ. Chem. Eng.* **2022**, *10*, 107296. [CrossRef]

33. Konopacka-Łyskawa, D. Synthesis Methods and Favorable Conditions for Spherical Vaterite Precipitation: A Review. *Crystals* **2019**, *223*, 223. [CrossRef]

34. Yao, H.; Ge, J.; Mao, L.B.; Yan, Y.X.; Yu, S.H. Artificial Carbonate Nanocrystals and Layered Structural Nanocomposites Inspired by Nacre: Synthesis, Fabrication and Applications. *Adv. Mater.* **2014**, *26*, 163–188. [CrossRef]

35. Naka, K.; Tanaka, Y.; Chujo, Y. Effect of anionic starbust dendrimers on the crystallization of $CaCO_3$ in aqueous solution: Size control of spherical vaterite particles. *Langmuir* **2002**, *18*, 3655–3658. [CrossRef]

36. Kirboga, S.; Öner, M. Application of experimental design for the precipitation of calcium carbonate in the presence of biopolymer. *Powder Technol.* **2013**, *249*, 95–104. [CrossRef]

37. Boyjoo, Y.; Pareek, V.K.; Liu, J. Synthesis of micro and nano-sized calcium carbonate particles and their applications. *J. Mater. Chem. A* **2014**, *2*, 14270–14288. [CrossRef]

38. Liu, X.; Wang, B.; Zhang, Z.; Pan, Z.; Cheng, H.; Cheng, F. Glycine-induced synthesis of vaterite by direct aqueous mineral carbonation of desulfurization gypsum. *Environ. Chem. Lett.* **2022**, *20*, 2261–2269. [CrossRef]

39. Kim, G.; Kim, S.; Kim, M.-J. Effect of sucrose on CO_2 storage, vaterite content, and CaCO3 particle size in indirect carbonation using seawater. *J. CO2 Util.* **2022**, *57*, 101894. [CrossRef]

40. Kontoyannis, C.G.; Vagenas, N.V. Calcium carbonate phase analysis using XRD and FT-Raman spectroscopy. *Analyst* **2000**, *125*, 251–255. [CrossRef]

41. Azarian, M.H.; Sutapun, W. Tuning polymorphs of precipitated calcium carbonate from discarded eggshells: Effects of polyelectrolyte and salt concentration. *RSC Adv.* **2022**, *12*, 14729–14739. [CrossRef] [PubMed]

42. Rodriguez-Blanco, J.D.; Shawa, S.; Benning, L.G. The kinetics and mechanisms of amorphous calcium carbonate (ACC) crystallization to calcite, via vaterite. *Nanoscale* **2011**, *3*, 265–271. [CrossRef] [PubMed]

43. Zhao, L.; Zhang, G.; Wang, M.; Zhen, S. Preparation of high-purity vaterite CaCO3 from lead-zinc tailings. *Sustain. Chem. Pharm.* **2022**, *29*, 100835. [CrossRef]

44. Song, X.; Cao, Y.; Bu, X.; Luo, X. Porous vaterite and cubic calcite aggregated calcium carbonate obtained from steamed ammonia liquid waste for Cu_{2+} heavy metal ions removal by adsorption process. *Appl. Surf. Sci.* **2021**, *536*, 147958. [CrossRef]

45. Song, X.; Weng, C.; Cao, Y.; Kong, H.; Luo, X. Facile synthesis of pure vaterite using steamed ammonia liquid waste and ammonium carbonate without additives via simple mechanical mixing. *Powder Technol.* **2021**, *386*, 361–371. [CrossRef]

46. Zhang, J.; Dong, C.H.; Sun, Y.Z.; Yu, J. Mechanism of Magnesium's Influence on Calcium Carbonate Crystallization: Kinetically Controlled Multistep Crystallization. *Cryst. Res. Technol.* **2018**, *53*, 1800075. [CrossRef]

47. Mejri, W.; Salah, I.B.; Tlili, M.M. Speciation of Fe(II) and Fe(III) efect on $CaCO_3$ crystallization. *Cryst. Res. Technol.* **2015**, *3*, 236–243. [CrossRef]

48. Szczes, A.; Chibowski, E.; Hołysz, L. Influence of ionic surfactants on the properties of freshly precipitated calcium carbonate. *Colloids Surf. A Physicochem. Eng. Asp.* **2007**, *297*, 14–18. [CrossRef]

49. Gehrke, N.; Colfen, H.; Pinna, N.; Antonietti, M.; Nassif, N. Superstructures of Calcium Carbonate Crystals by Oriented Attachment. *Cryst. Growth Des.* **2004**, *5*, 1317–1319. [CrossRef]